

A Global Probability-of-Fire (PoF) Forecast

Joe Ramu McNorton¹, Francesca Di Giuseppe², Ewan Mark Pinnington³, Matthew Chantry², and Chris Barnard²

¹European Centre for Medium-Range Weather Forecasts

²ECMWF

³National Center for Earth Observation, Department of Meteorology, University of Reading

January 16, 2024

Abstract

Accurate wildfire forecasting can inform regional management and mitigation strategies in advance of fire occurrence. Existing systems typically use fire danger indices to predict landscape flammability, based on meteorological forecasts alone, often using little or no direct information on land surface or vegetation state. Here, we use a vegetation characteristic model, weather forecasts and a data-driven machine learning approach to construct a global daily ~9 km resolution Probability of Fire (PoF) model operating at multiple lead times. The PoF model outperforms existing indices, providing accurate forecasts of fire activity up to 10 days in advance, and in some cases up to 30 days. The model can also be used to investigate historical shifts in regional fire patterns. Furthermore, the underlying data driven approach allows PoF to be used for fire attribution, isolating key variables for specific fire events or for looking at the relationships between variables and fire occurrence.

Hosted file

982518_0_art_file_11701667_s62bjg.docx available at <https://authorea.com/users/713243/articles/697596-a-global-probability-of-fire-pof-forecast>

Hosted file

982518_0_supp_11701670_s5vfcp.docx available at <https://authorea.com/users/713243/articles/697596-a-global-probability-of-fire-pof-forecast>

1
2
3
4
5
6
7
8
9
10
11
12

A Global Probability-of-Fire (PoF) Forecast

J. R. McNorton¹, F. Di Giuseppe¹, E. Pinnington¹, M. Chantry¹, C. Barnard¹

¹European Centre for Medium-Range Weather Forecasts, Reading, UK.

Corresponding author: Joe McNorton (joe.mcnorton@ecmwf.int)

Key Points:

- A data-driven model informed by satellite observations and an Earth System Model provides accurate fire forecasts upto 10 days in advance.
- The probability of fire forecast is implemented operationally in a numerical weather prediction model to provide real-time forecasts.
- Fire attribution is demonstrated and can be used for specific fire events or historical analysis.

13 **Abstract**

14 Accurate wildfire forecasting can inform regional management and mitigation strategies in advance of fire
15 occurrence. Existing systems typically use fire danger indices to predict landscape flammability, based on
16 meteorological forecasts alone, often using little or no direct information on land surface or vegetation state. Here,
17 we use a vegetation characteristic model, weather forecasts and a data-driven machine learning approach to
18 construct a global daily ~9 km resolution Probability of Fire (PoF) model operating at multiple lead times. The PoF
19 model outperforms existing indices, providing accurate forecasts of fire activity up to 10 days in advance, and in
20 some cases up to 30 days. The model can also be used to investigate historical shifts in regional fire patterns.
21 Furthermore, the underlying data driven approach allows PoF to be used for fire attribution, isolating key variables
22 for specific fire events or for looking at the relationships between variables and fire occurrence.

23 **Plain Language Summary**

24 Wildfires have widespread effects on local ecosystems, communities, air quality, and global atmospheric conditions.
25 Accurate wildfire forecasts can be used by local communities and agencies to manage and respond to wildfires
26 effectively. As such, it is essential these predictions are not only accurate but are accessible in real-time and provide
27 sufficient advanced notice to ensure successful actions can be taken. To achieve this we have developed a
28 forecasting system that combines satellite observations, weather forecasting and vegetation characteristics using
29 machine learning. Tested on historical data and operated in real-time, our model provides a global daily wildfire
30 forecast with a 9 km resolution, predicting the likelihood of fires up to 30 days in advance. The model outperforms
31 existing fire danger forecasts when evaluated against satellite observations of active fires. It can also identify key
32 drivers which result in the occurrence of fire. Finally, it not only offers real-time forecasts but can be used to help
33 investigate past fire events, understand their causes, and predict wildfire activity over longer climate timescales.

34 **1 Introduction**

35 Wildfires play a crucial role in the Earth system influencing ecosystems, communities, air quality and the carbon
36 cycle (Moritz et al., 2014). Catastrophic wildfire effects include agricultural and infrastructure damage, destruction
37 of wild habitats and loss of both animal and human life. Wildfire management and prevention strategies can help
38 mitigate some of these effects, but these depend on accurate forecasts of fire occurrence.

39
40 The stochastic nature of wildfire ignitions makes forecasting specific events extremely challenging. Beyond
41 ignitions, the two remaining prerequisites for fire activity, fuel and moisture, are intricately linked to the land
42 surface state. Therefore, it is feasible that a probabilistic fire forecast can be achieved with a reasonable degree of
43 accuracy by considering the land surface state. Historically fire danger forecasts have been derived by linking
44 weather variables with fire activity to produce an index, the most widely used is the Fire Weather Index (FWI, Van
45 Wagner, 1974). The FWI provides only an approximate estimation of the state of fuel moisture based on the impact
46 of meteorological conditions on a fixed fuel bed typical of the Boreal forests. It neglects to account for the moisture
47 state of living vegetation, the type of vegetation or the abundance of fuel available to burn in the event of a fire. As a
48 result, the FWI overestimates fire danger in fuel and sometimes high moisture domains (Di Giuseppe, 2023).
49 Furthermore, interpretation of FWI values is domain specific as it does not directly translate into the probability of
50 fire.

51
52 Previously, process-based models have attempted to describe fire danger based on the land surface, and to a degree
53 the atmospheric state (e.g. Thonicke et al., 2010). The complexity in the relationship between vegetation and fire
54 occurrence make probabilistic wildfire occurrence difficult to describe using process-based modelling. Recently, the
55 use of data driven methods has emerged as an option to overcome the complexity of describing the underlying
56 processes (e.g. Zhang et al., 2021; Kondylatos et al., 2022, Zhu et al., 2022). A comparison between the two
57 methods by Leuenberger et al. (2018) showed several advantages to using the data-driven approach. Data-driven
58 methods are effective when required input observations are available; however, this is not an option when generating
59 future forecasts. Here, we propose a global probabilistic fire forecast which derives key input variables using state-
60 of-the-art numerical weather prediction (NWP) and land surface modelling and then uses a data-driven approach to
61 estimate the likelihood of fire occurrence on a given day for multiple forecast lead times.

62 2 Materials and Methods

63 We propose a modelling framework to provide a forecast Probability of Fire (PoF) on a given day within a 9 km by
64 9 km grid cell using data-driven statistical methods informed by observations and an Earth system model. As input,
65 we used analysis output from the Integrated Forecast System (IFS), which is the operational NWP system used by
66 the European Centre for Medium-Range Weather Forecasts (ECMWF). The IFS is initialised every 6-hours and
67 provides both NWP and land surface output at hourly out to seasonal forecast ranges. As time varying NWP input,
68 we used daily mean precipitation, 10m wind speed, 2m dew point temperature and 2m temperature taken from the
69 re-analysis product (ERA-5 Land, Muñoz-Sabater et al., 2021), which assimilates observations to improve accuracy
70 of modelled variables. Fuel characteristics used as input were computed following McNorton and Di Giuseppe
71 (2023) using additional land surface variables including vegetation cover, vegetation type, soil moisture at 4
72 different levels, surface pressure and skin temperature. These characteristics include both dead and live fuel load and
73 moisture, which were further divided into wood and foliage components. Furthermore, as input we used time-
74 varying Leaf Area Index (LAI) for both low and high vegetation, based on satellite observations, as described by
75 Boussetta and Balsamo (2021). The remaining input variables were taken from static land cover maps for urban
76 fraction (McNorton et al., 2023), orography and vegetation type (Boussetta et al., 2021). This resulted in a total of
77 17 input features, 4 directly from NWP, 7 from fuel characteristics, 2 LAI estimates and 4 land static surface maps.

78
79 Using the inputs described, we trained two tree-based data-driven models, Random Forest (RF, Breiman, 2001) and
80 Extreme Gradient Boosting (XGBoost, Chen & Guestrin, 2016), and interpret the output of the classification models
81 as estimates of the likelihood of fire occurrence. A probabilistic forecast approach was chosen given a binary
82 classification would almost always return a no fire event as the probability values would fall below 50%. Both RF
83 and XGBoost methods are supervised algorithms which involve training an ensemble of decision trees to resolve the
84 classifier problem. The RF approach randomly subsamples the data to train individual trees which are then clustered
85 to form the final decision tree model. XGBoost improves the performance of decision trees by sequentially adding
86 models to correct errors made by previous ones and uses regularisation techniques to prevent overfitting. The
87 optimisation of XGBoost makes it computationally efficient when compared to RF. In the classifier approach we
88 define a positive hit as an active fire detection within the 9km x 9km grid cell on a given day.

89
90 For training, we used daily data from the MODIS Collection 6 and 6.1 Active Fire Dataset between 2010 and 2014
91 (Giglio et al., 2020). The dataset uses retrievals in the mid-infrared and a contextual algorithm (Giglio et al., 2016).
92 The dataset likely misses many fire events as it only provides a snapshot at the overpass time, missing fires
93 occurring before and after the overpass window. Furthermore, spurious detections are also likely for non-wildfire
94 events e.g. gas flaring. Where possible, these detections were removed using a spurious signal mask. To align with
95 input data, we gridded the active fire data to the same resolution (~9 km, daily), resulting in 2.9x10¹⁰ data points
96 (5136 longitude, 2560 latitude, 2191 days) which was too large for training either model given the computing
97 resources available. To reduce the training data size whilst maintaining a representation of spatial and temporal
98 variability in the trained model we first removed all non-land points from the dataset. Of the remaining points we
99 randomly sampled 5% of the data for training, resulting in 3x10⁸ data points for training. The RF training had
100 increased memory demands, for this only 2% of the data was sampled. The resulting models predict the probability
101 that at least one MODIS active fire detection would be made within a ~9 km grid cell for a given day, which we
102 assume to be a proxy for the probability of fire occurrence.

103
104 The trained model was then used at multiple forecast lead times using operational NWP forecasts from the IFS.
105 These were simulated from hourly output averaged daily to provide 1 to 30 day forecasts. The regional and global
106 skill of each forecast lead time was evaluated against a monthly climatology of the XGBoost model output.
107 Remaining input features can either be taken from observations or model predictions, here we used a combination of
108 both. For example, operationally LAI is taken from a climatology as forecast LAI is not available in real-time;
109 however, for historical evaluation we used observation-based LAI from the CONFESS Project (Boussetta and
110 Balsamo 2021). With further model development more variables will be derived in the model forecast with the aim
111 of improving forecast skill.

112 3 Results

113 The XGBoost and RF trained models were evaluated globally using daily MODIS active fire observations for a
114 period independent from the training, 2015-2019. The resulting models were also compared with a monthly

115 climatology derived using the XGBoost method for the entire 2015-2019 period to evaluate their relative forecast
116 performance. Given the binary classifier approach resulted in few positive results, as the PoF on a given day for a
117 given grid cell was rarely greater than 50 %, typical evaluation metrics, such as the confusion matrix, were not
118 possible. Instead, we focused on the probabilistic skill of the model.

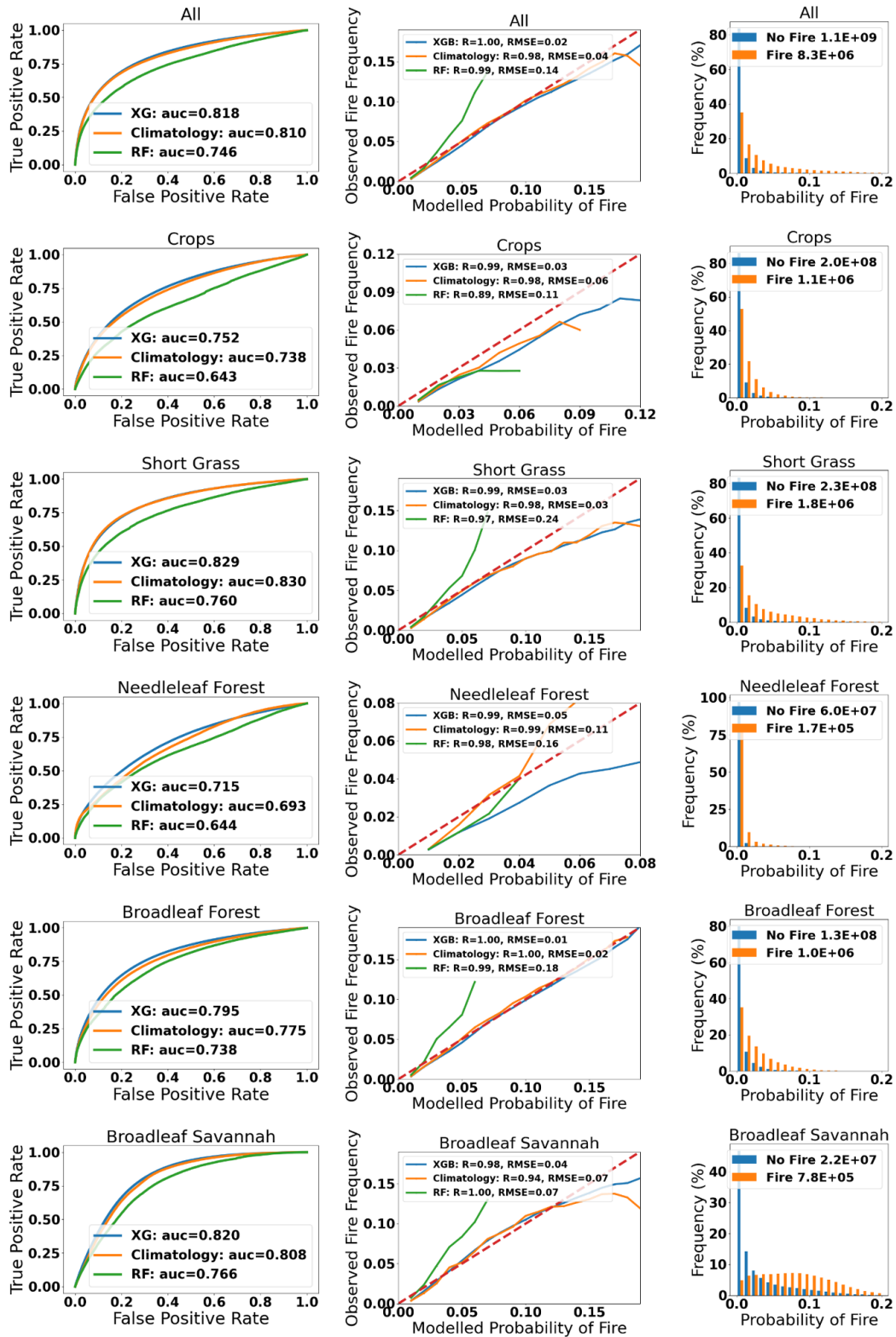
119 **3.1 Probability of Fire (PoF) Evaluation**

120 A receiver operating characteristic (ROC) curve was used to show the performance of the models by comparing the
121 probabilistic false positive rate with the true positive rate for land points at ~9 km resolution at daily resolution
122 between 2015 and 2019 (Figure 1). The large number of values which occupy extremely low probability space, for
123 example in desert regions, were removed by only including probabilities greater than 0.1 %. The area under the
124 ROC curve (AUC) provides a metric for assessing the skill of the model in distinguishing between a positive fire
125 event or no fire event, with a score of 1 illustrating a perfect model. Results show, when considering all vegetation
126 types, the XGBoost method produces the highest AUC score, 0.818, higher than the RF method, 0.746, and the
127 monthly climatology based on XGBoost, 0.810. By removing probabilities less than 0.1% these scores are
128 artificially decreased. For specific vegetation types XGBoost model skill is high, for example short grass (AUC:
129 0.829) and broadleaf savannah (AUC: 0.820); however, it is noticeably lower for needleleaf forests (AUC: 0.719).
130 The RF (AUC: 0.644) only slightly outperforms a random forecast (AUC: 0.5) over needleleaf forests, indicating
131 low model skill.

132
133 A reliability curve, which is a measure of how well the predicted probability reflects the true probability of fire
134 occurrence, was generated by binning predicted fire activity into one percentile bins from 0 % up to 20 % (Figure 1).
135 The frequency of predictions above 20 % become too small to be considered as a reliable metric, although any value
136 above this can be considered to represent extreme fire danger. Model data was evaluated against observed fire
137 frequency based on all points within the target bin, where an ideal model would follow a 1-to-1 line. Across all
138 vegetation types the highest model skill is found when using XGBoost with RF providing reasonable skill at low fire
139 probabilities but underestimating fire occurrence as PoF increases. Therefore, the RF model is unsuitable for more
140 extreme fire events where fire danger is considered high. XGBoosts produced reliable forecast probabilities for all
141 vegetation types when compared with both RF and the XGBoost climatology, although for broadleaf savannah,
142 crops and short grass the model overpredicts PoF when values exceed 10%, which rarely occurs. For needleleaf
143 forests the XGBoost model offers reliable prediction when PoF is <5 %, after which the model overpredicts PoF;
144 however, the frequency of occurrence for predictions about 5 % is very low. For broadleaf forests the model
145 accurately predicts PoF continuously up to the 20 % threshold considered. The relative improved performance when
146 compared with the XGBoost climatology shows modelling time specific PoF results in a more reliable forecast.

147
148 For qualitative purposes we present normalised histograms of modelled PoF when fires are and are not detected, these
149 show the distribution of observed active fires are skewed toward higher probabilities (Figure 1). When considering
150 points with PoF larger than 0.1 %, we find 35 % of all fires occur at probabilities between 0.1% and 1%; which is
151 unsurprising considering these make up over 80 % of all points.

152



153
154
155
156
157
158

Figure 1. Receiver operating characteristic curves for a daily XGBoost model (blue), the XGBoost model climatology (orange) and a daily Random Forest model (green) of active fires using ERA-5 Land input evaluated against MODIS observations for all land points globally between 2015 and 2019 for multiple vegetation types (left column). The same data represented using reliability curves (middle column). Normalised histograms of the modelled probability of fire divided between observed non-fire and fire detections for all vegetation types (right column).

159

160

3.2 PoF Forecast Skill

161 The predictive capability of the PoF model for operational forecasting is dependent on the accuracy of input
162 forecasts. To evaluate model skill, we used input from day- 1, 3, 10 and 30 forecast times and compared the results
163 with observed active fire from MODIS for the target day between 2015 and 2019. The model setup was as
164 previously described, however operational NWP forecasts provided input to the model, which differ from the ERA-5
165 Land data used to train the model (Muñoz-Sabater et al., 2021). Whilst both input datasets were used at the same
166 spatiotemporal resolution (daily average and ~9 km) there are two main differences. ERA-5 Land assimilates more
167 observations, providing a more realistic representation of the land and atmosphere state relative to the operational
168 forecast. However, ERA-5 (Hersbach et al., 2020) atmospheric data is used as boundary conditions for ERA-5 Land,
169 which is at a coarser resolution (~25 km) than operational forecast data (~9 km). A further consideration is whilst
170 operational high-resolution simulations provided input for 1-, 3- and 10-day forecasts, the production of the 30-day
171 forecast used the operational extended-range forecast simulated at ~36 km resolution, which likely limits model
172 skill.

173

174 Given model performance previously assessed, we only evaluated the XGBoost model, details of which are given by
175 Supporting Information S1. The ROC curve and reliability curve for multiple forecast lead times show similar model
176 skill between day 1 and day 10 (Figure 2). 30-day forecasts failed to outperform the climatology of the 30-day
177 XGBoost forecast. The decrease in model skill was most evident when forecasting relatively rare high PoF values
178 (>0.05), the frequency of which are reduced in the climatology because of averaging multi-year values. This
179 compensates for the typical over-prediction of high probability events by the model at all lead times. The reduced
180 resolution and declining NWP skill at longer lead times further explains this reduction in PoF skill for 30-day
181 forecasts. These results show that whilst model skill may be present in the 30-day forecast it is difficult to quantify.

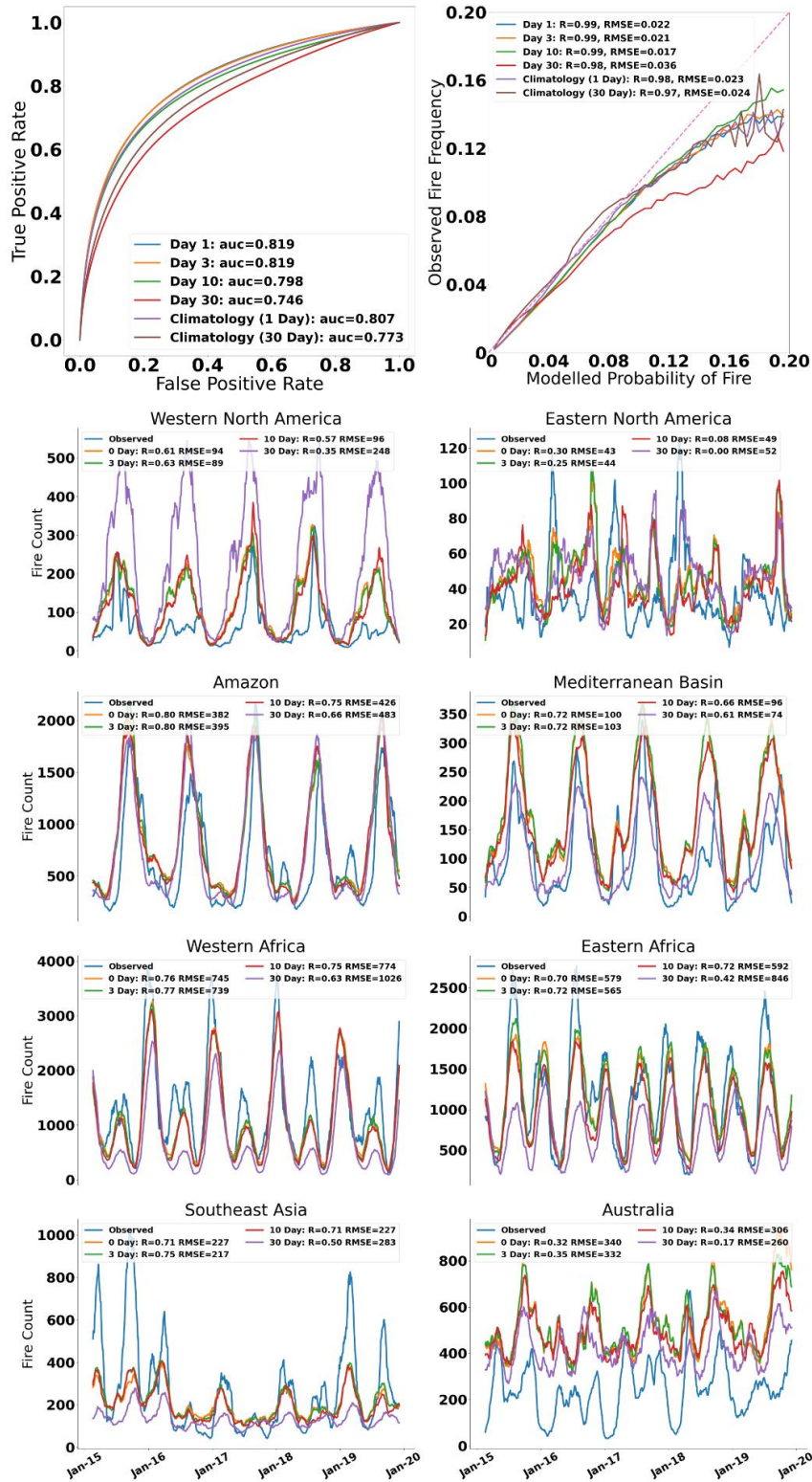
182

183 Improved forecast skill could be attained by training lead-time specific models which would overcome model bias
184 which emerges at longer forecast times. If such models were implemented, it would be recommended they were
185 retrained with each new model cycle to ensure consistency between training and operational input. Currently, we
186 have trained the model using the most realistic input variables available, ERA-5 Land (Muñoz-Sabater et al., 2021),
187 hence biases from the operational forecast may limit model skill. These biases are expected to reduce as the model
188 forecast continues to improve toward closer alignment with ERA-5 Land.

189

190 To evaluate regional skill at different lead times we compared the observed total fire count from MODIS
191 observations gridded to 9km resolution between 2015 and 2019 with our model forecasts for eight fire prone regions
192 defined by Giorgi and Franciso (2000). The summed probabilities over all ~9 km grid cells within a domain were
193 considered representative of the predicted total fire count (Figure 2). Regions with well defined fire seasons
194 (Western North America, Amazon, Western and Eastern Africa and the Mediterranean) were well represented at all
195 forecast lead times, although the maximum amplitude of fire counts for the Western North America fire season was
196 typically overestimated, particularly for the 30-day forecasts. A similar overestimation in modelled fire activity was
197 observed in Australia, although the timing of peak fire activity was typically in good agreement with observations.
198 The interannual variability in regions with seasonal fire were also well represented, e.g. Western Africa.

199

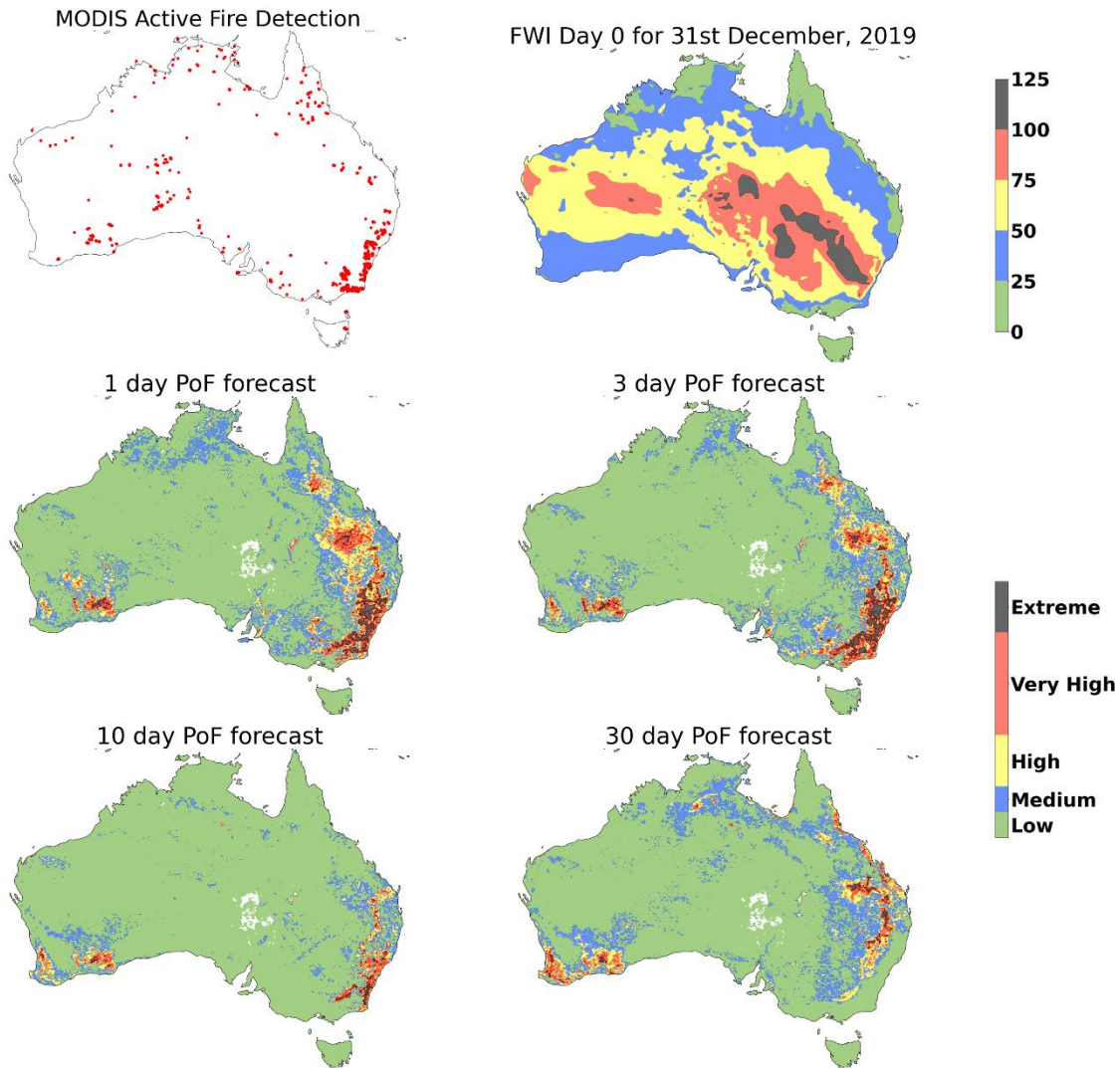


200
201
202
203
204
205

Figure 2. Receiver operating characteristic curves for daily PoF model at multiple lead times and monthly mean PoF model climatologies using input from the IFS evaluated against MODIS active fire observations for all ~9 km land points globally between 2015 and 2019 (top left). The same data represented using reliability curves (top right). Timeseries of 5-day average active fire counts at ~9km resolution from MODIS active fire observations compared with PoF model at multiple lead times. Also displayed is the R-value and RMSE for each forecast lead time (bottom three rows).

206
 207
 208
 209
 210
 211
 212
 213
 214
 215
 216
 217
 218
 219

The model capability to accurately represent spatial variability in fire activity at various lead times was limited by NWP skill. To illustrate this, we show the predictive skill of PoF during the peak of the 2019/2020 bushfire season in Australia, one of the largest in recorded history (Deb et al., 2020). As a case study we selected the 31st of December when most of the active fires were in New South Wales in the southeast of the country (Figure 3). The examples shown were made using the operational version of the model, which bins PoF values into 5 fire danger categories, low (<0.5 %), medium (0.5-1.0 %), high (1-2 %), very high (2-4 %) and extreme (> 4 %). Results highlight the spatial accuracy provided by forecasts out to 10-days and show some regional agreement between 30-day forecasts and fire activity. The lack of representation of vegetation in the FWI was evident by the high values produced in the sparsely vegetated central Australian regions. The FWI shown was not subject to forecast errors as it was derived at the analysis timestep, providing a now-forecast without any lead time. Despite this, it still underperformed relative to the PoF model at all forecast times, illustrating the improved predictive skill of the model.



220
 221
 222
 223
 224
 225

Figure 3. Active fire detection map over Australia from MODIS gridded to 9km resolution for 31st December 2019 (top left). The Fire Weather Index (FWI) using analysis forcing for the same date (top right). Probability of Fire (PoF) model forecast using 1-day (middle left), 3-day (middle right), 10-day (bottom left) and 30-day (bottom right) lead times from the Integrated Forecasting System (IFS) for the same date.

226

3.3 Fire Attribution

227 Several of the 17 input features of the PoF model were partially correlated; however, given they were features which
228 were not fully correlated, were readily available and over-fitting is unlikely given the high volume of training data,
229 we opted to keep all variables to maximise model performance. However, given there was partial correlation,
230 traditional feature selection methods make attribution difficult to interpret, instead we interpreted the results by
231 looking at both Shapley values (SHAP) and the interaction of those values (Lundberg & Lee, 2017). The SHAP
232 value denotes the importance of any given feature in a model, with a positive SHAP value indicating a positive
233 impact on the model prediction and a negative SHAP value a negative impact on the model prediction.

234

235 At a global scale we find 2m dewpoint temperature to be the most important feature. This is, in part, a result of it
236 being strongly correlated with only one other variable, 2m temperature (Figure 4). In contrast the individual
237 importance of variables relating to fuel load and moisture was relatively low as they include multiple well correlated
238 variables. When those variables are combined their importance becomes evident.

239

240 Several interesting features emerged from the SHAP calculations, for example increased 2m dewpoint temperature
241 displayed increased SHAP values. However, increased 2m temperature resulted in decreased SHAP values in
242 response to the uncorrelated component in the relationship between 2m temperature and dewpoint temperature.
243 Therefore, for a given 2m dewpoint temperature, an increasing 2m temperature typically acts to reduce the PoF
244 (Figure 4). If 2m dewpoint temperature were removed as an input variable, increased 2m temperature would result in
245 an increased SHAP value. For other variables non-linear relationships were identified, for example, SHAP values
246 for precipitation followed an exponential decay function, which is expected as beyond a certain precipitation rate the
247 flammability of the fuel remains unchanged. As fuel load increased the SHAP values increased, however, the
248 contribution of fuel load to PoF was dependent on the abundance of other fuel types, as expected. For high fuel
249 loads the contribution of each variable generally became smaller as the remaining 3 fuel load variables compensated
250 to increase PoF in these fuel rich regimes, whilst the combined SHAP value contribution from all 4 fuel load
251 variables remained relatively unchanged. The relationship between fuel loads and their respective SHAP values was
252 also partially dependent on moisture content.

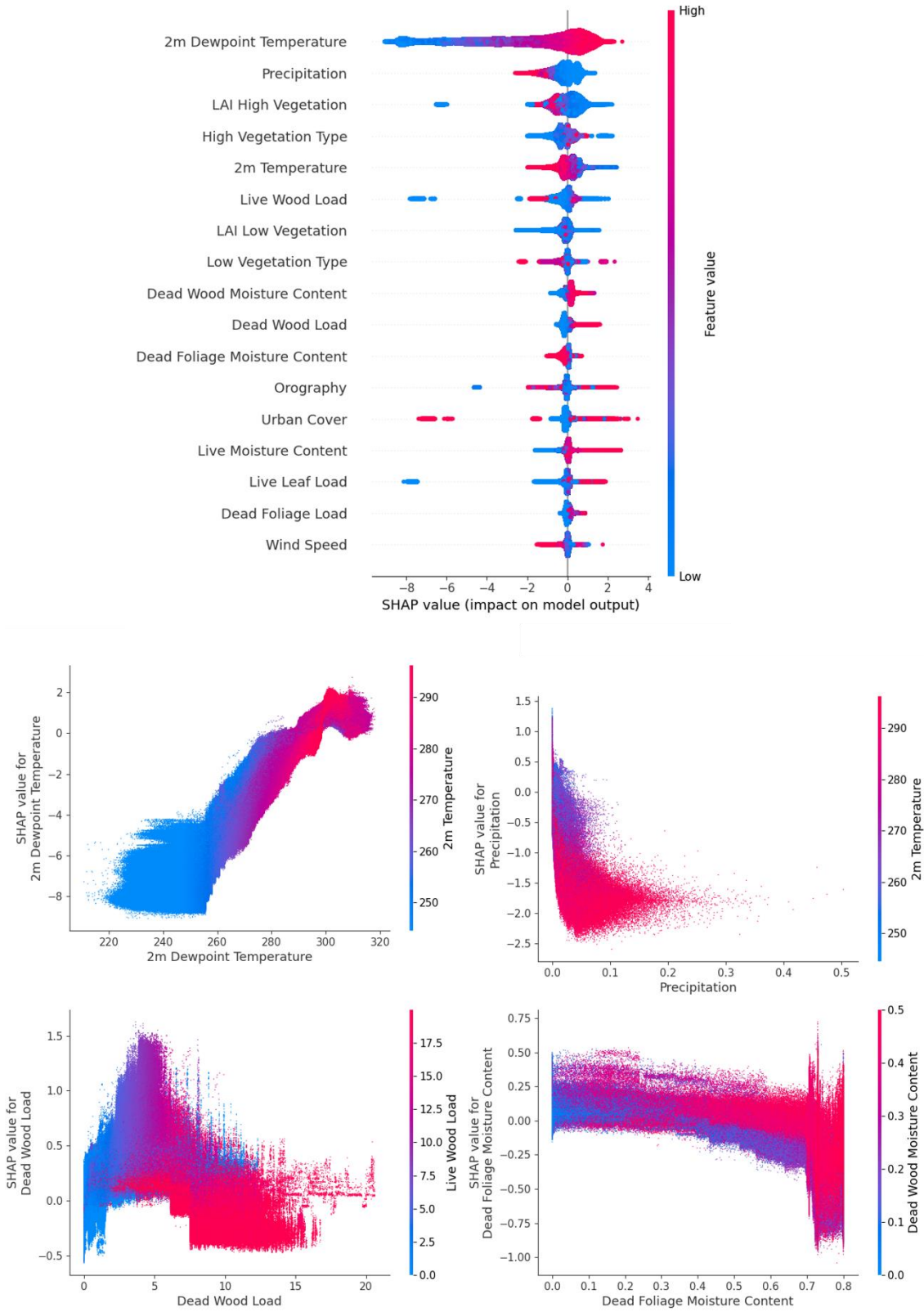
253

254 SHAP values for fuel moisture content, a commonly used variable for fire danger forecasting (Yebra et al., 2013),
255 typically showed a step change decrease above a certain threshold. Similar thresholds are reported in the literature
256 for both DFMC and LFMC. Argañaraz et al. (2018), supported by the subsequent study of Rao et al. (2023), found
257 LFMC thresholds for wildfire ignition of 55 % to 106 %. Whilst Masinda et al. (2020) and Wotton (2009) found
258 DFMC ignition thresholds of 10-40 % and 17 %, respectively, with variability for both DFMC and LFMC
259 thresholds being controlled by vegetation type. Here, DFMC was separated between fine and coarse fuels with
260 average ignition thresholds, based on SHAP values, of 42 % and 70 %, respectively, when averaged across all
261 vegetation types. The resulting DFMC threshold was therefore dependent on the allocation of dead fuel between fine
262 and coarse fuel. This represents the point above which the SHAP values related to DFMC noticeably decrease but as
263 previously mentioned the result of the correlation between variables mean this does not necessarily represent a
264 realistic ignition threshold. We found average LFMC ignition thresholds were difficult to distinguish because they
265 are vegetation dependent but also vary as a function of phenology. For example, during the growth season, LFMC is
266 usually high whilst vegetation is active; however, these high LFMC values occur during active fire seasons.

267

268 The attribution for fire activity performed here, in part, neglects other controlling influences on fire activity, e.g.
269 ignition and suppression. However, this evaluation tool could still be used at climate time scales to identify regime
270 shifts in the driving variables of fire activity (e.g. Kelley et al., 2019). Furthermore, spatial patterns and plant
271 specific attribution can provide insight into regional fire activity; however, that is beyond the scope of this study and
272 will be investigated further in a follow-up study.

273



274
275
276
277
278

Figure 4. Ordered Shapley values (SHAP) for 17 features used to inform the XGBoost fire model, where colour indicates feature value and dots represent individual predictions (top). Dependency plots displaying the change in feature value with respect to the SHAP value, where the colour indicates a second feature value given by the colourbar and dots represent individual predictions globally for all times (bottom).

279 5 Conclusions

280 The stochastic nature of wildfire activity limits predictability of specific events; however probabilistic forecasting
 281 has previously been used to provide a representation of fire danger (e.g. Di Giuseppe, 2023). Here, we move beyond
 282 conventional fire danger indices to produce a probability of fire, PoF, forecast at various lead times using a data-
 283 driven model informed by a combination of NWP variables, land surface modelling and observations. The intention
 284 is to provide a global high-resolution daily forecast which can be utilised for wildfire planning and management
 285 strategies. As the model was trained using observed fire activity it encompasses, to an extent, processes which are
 286 difficult to represent in physical-based models, for example the human-drivers for fire activity. The model was
 287 trained globally at ~9 km resolution to provide a daily grid cell specific PoF, an easily interpretable metric. The
 288 model can be simulated at any NWP lead-time and model skill is demonstrated up to 10 days in advance. Model
 289 skill beyond this may be limited by the degraded resolution of extended-range forecasts, it is recommended that
 290 high-resolution forecasts (~9 km) be used for all forecast lead-times when available. Alternatively, lead-time
 291 specific models could be trained to account for forecast biases. Although not explored in this study, the modelling
 292 framework could easily be adapted to provide a forecast probabilistic spread using input data from the operational
 293 NWP ensemble (Leutbecher and Palmer, 2008).

294
 295 Two versions of the data-driven model were trained, using Random Forest and XGBoost. XGBoost provided better
 296 skill, although lower memory requirements meant it was trained on a large sample of data. Furthermore, software
 297 packages for attribution are readily available with XGBoost. The skill in predicted fire activity in certain vegetation
 298 types, e.g. Needleleaf Forest, was relatively low, although some skill was still found. The model provided a high
 299 forecast skill for other vegetation types, e.g. Broadleaf Savannah. The model skill at predicting actual fire activity is
 300 limited by the accuracy of the observing systems available (Wooster *et al.*, 2021).

301
 302 As more variables become available for forecast input in the future, e.g. prognostic LAI, model skill is expected to
 303 further improve, as currently input variables limit the skill at longer lead times. Furthermore, the addition of input
 304 variables that control ignition, whether human or lightning activity, are expected to further improve model skill.
 305 Currently, variables directly correlated with fire activity have been used as input to the model; however, it is feasible
 306 that by performing regional or grid point specific training will result in improved model performance by indirectly
 307 representing processes not included in our input. The model, as described here, is used operationally at ECMWF. It
 308 provides a real-time 10-day fire probability forecast and is available through the ECCharts web platform hosted at
 309 <https://eccharts.ecmwf.int>.

310
 311 The attribution of input variables to the PoF can be made using evaluation tools, such as SHAP (Lundberg and Lee,
 312 2017). Here we use these to identify relationships between specific variables and fire danger. Whilst these are
 313 sometimes simple linear fits, they are often more complex involving either threshold values or non-linear
 314 relationships. These attribution tools could be used to identify causes of extreme fire events and to evaluate controls
 315 on specific fire regimes both in the real-time and at climate timescales.

316 Acknowledgments

317 This work was funded by the Copernicus Emergency Management Service contract no. 942604 between the Joint
 318 Research Centre and ECMWF.

319

320 Open Research

321 Input meteorological data for training the PoF model presented here is taken from the ERA5-Land dataset openly
 322 available through the Copernicus Climate Data store (<https://doi.org/10.24381/cds.e2161bac>). Full details of input
 323 fuel data is available in McNorton and Di Giuseppe (2023) and will be shortly be released in the ECMWF Climate
 324 Data store. Currently the data is available to ECMWF registered users for direct download: for fuel load this is
 325 available at: http://cemsfire.copernicus-climate.eu/FUEL_DATA/ECMWF-Fuel-Characteristics_V1/Fuel-Load/<YYY>/FUEL_MAP<YYYY><MM>.nc, live fuel moisture is available at : http://cemsfire.copernicus-climate.eu/FUEL_DATA/ECMWF-Fuel-Characteristics_V1/Fuel-Moisture/Live/<YYY>/LFMC_MAP<YYYY><MM>.nc and dead fuel moisture is available at :
 326
 327
 328
 329 http://cemsfire.copernicus-climate.eu/FUEL_DATA/ECMWF-Fuel-Characteristics_V1/Fuel-

330 [Moisture/Dead/<YYY>/DFMC_MAP <YYYY> <MM>.nc](#). Operational model output is available to registered
 331 users through the web platform, ECCharts (<https://eccharts.ecmwf.int>) and will soon be made openly available at
 332 <https://charts.ecmwf.int/>.

333

334 **References**

335 Argañaraz, J. P., Landi, M. A., Scavuzzo, C. M., & Bellis, L. M. (2018). Determining fuel moisture thresholds to
 336 assess wildfire hazard: A contribution to an operational early warning system. *PLOS ONE*, *13*(10), e0204889-
 337 <https://doi.org/10.1371/journal.pone.0204889>

338 Boussetta, S. and Balsamo, G. (2021). *Vegetation dataset of Land Use/Land Cover and Leaf Area Index*. [online]
 339 *CONFESS-H2020*. Available at: <https://confessh2020.files.wordpress.com/2021/08/confess-d1-1-v1-0-.pdf>
 340 [Accessed 21 Aug. 2023].

341 Boussetta, S., Balsamo, G., Arduini, G., Dutra, E., McNorton, J., Choulga, M., Agustí-Panareda, A., Beljaars, A.,
 342 Wedi, N., Muñoz-Sabater, J., de Rosnay, P., Sandu, I., Hadade, I., Carver, G., Mazzetti, C., Prudhomme, C.,
 343 Yamazaki, D., & Zsoter, E. (2021). ECLand: The ECMWF Land Surface Modelling System. *Atmosphere*, *12*(6).
 344 <https://doi.org/10.3390/atmos12060723>

345 Breiman, L. (2001). Random Forests. *Machine Learning*, *45*(1), 5–32. <https://doi.org/10.1023/A:1010933404324>

346 Chen, T., & Guestrin, C. (2016). XGBoost: A Scalable Tree Boosting System. *Proceedings of the 22nd ACM*
 347 *SIGKDD International Conference on Knowledge Discovery and Data Mining*, 785–794.
 348 <https://doi.org/10.1145/2939672.2939785>

349 Deb, P., Moradkhani, H., Abbaszadeh, P., Kiem, A. S., Engström, J., Keellings, D., & Sharma, A. (2020). Causes of
 350 the Widespread 2019–2020 Australian Bushfire Season. *Earth's Future*, *8*(11), e2020EF001671.
 351 <https://doi.org/https://doi.org/10.1029/2020EF001671>

352 Di Giuseppe, F. (2023). Accounting for fuel in fire danger forecasts: the fire occurrence probability index (FOPI).
 353 *Environmental Research Letters*, *18*(6), 064029. <https://doi.org/10.1088/1748-9326/acd2ee>

354 Giglio, L., Schroeder, W., & Justice, C. O. (2016). The collection 6 MODIS active fire detection algorithm and fire
 355 products. *Remote Sensing of Environment*, *178*, 31–41. <https://doi.org/https://doi.org/10.1016/j.rse.2016.02.054>

356 Giglio, L., Schroeder, W., Hall, J. and Justice, C. (2020). *MODIS Collection 6 Active Fire Product User's Guide*
 357 *Revision C*. [online]. Available at: https://modis-fire.umd.edu/files/MODIS_C6_Fire_User_Guide_C.pdf [Accessed
 358 21 Aug. 2023].

359 Giorgi, F., & Francisco, R. (2000). Evaluating uncertainties in the prediction of regional climate change.
 360 *Geophysical Research Letters*, *27*(9), 1295–1298. <https://doi.org/https://doi.org/10.1029/1999GL011016>

361 Hersbach, H., Bell, B., Berrisford, P., Hirahara, S., Horányi, A., Muñoz-Sabater, J., Nicolas, J., Peubey, C., Radu,
 362 R., Schepers, D., Simmons, A., Soci, C., Abdalla, S., Abellan, X., Balsamo, G., Bechtold, P., Biavati, G., Bidlot, J.,
 363 Bonavita, M., ... Thépaut, J.-N. (2020). The ERA5 global reanalysis. *Quarterly Journal of the Royal Meteorological*
 364 *Society*, *146*(730), 1999–2049. <https://doi.org/https://doi.org/10.1002/qj.3803>

- 365 Kelley, D. I., Bistinas, I., Whitley, R., Burton, C., Marthews, T. R., & Dong, N. (2019). How contemporary
 366 bioclimatic and human controls change global fire regimes. *Nature Climate Change*, 9(9), 690–696.
 367 <https://doi.org/10.1038/s41558-019-0540-7>
- 368 Leuenberger, M., Parente, J., Tonini, M., Pereira, M. G., & Kanevski, M. (2018). Wildfire susceptibility mapping:
 369 Deterministic vs. stochastic approaches. *Environmental Modelling & Software*, 101, 194–203.
 370 <https://doi.org/https://doi.org/10.1016/j.envsoft.2017.12.019>
- 371 Leutbecher, M., & Palmer, T. N. (2008). Ensemble forecasting. *Journal of Computational Physics*, 227(7), 3515–
 372 3539. <https://doi.org/https://doi.org/10.1016/j.jcp.2007.02.014>
- 373 Lundberg, S. M., & Lee, S.-I. (2017). A unified approach to interpreting model predictions. *Advances in Neural*
 374 *Information Processing Systems*, 30, 4765–4774. <https://doi.org/10.48550/arXiv.1705.07874>
- 375 Moritz, M. A., Batllori, E., Bradstock, R. A., Gill, A. M., Handmer, J., Hessburg, P. F., Leonard, J., McCaffrey, S.,
 376 Odion, D. C., Schoennagel, T., & Syphard, A. D. (2014). Learning to coexist with wildfire. *Nature*, 515(7525), 58–
 377 66. <https://doi.org/10.1038/nature13946>
- 378 Kondylatos, S., Prapas, I., Ronco, M., Papoutsis, I., Camps-Valls, G., Piles, M., Fernández-Torres, M. Á., &
 379 Carvalhais, N. (2022). Wildfire Danger Prediction and Understanding With Deep Learning. *Geophysical Research*
 380 *Letters*, 49(17). <https://doi.org/10.1029/2022GL099368>
- 381 Masinda, M. M., Li, F., Liu, Q., Sun, L., & Hu, T. (2021). Prediction model of moisture content of dead fine fuel in
 382 forest plantations on Maoer Mountain, Northeast China. *Journal of Forestry Research*, 32(5), 2023–2035.
 383 <https://doi.org/10.1007/s11676-020-01280-x>
- 384 McNorton, J. R. and Di Giuseppe, F.: A global fuel characteristic model and dataset for wildfire prediction,
 385 *EGUsphere* [preprint], <https://doi.org/10.5194/egusphere-2023-1984>, 2023.
- 386 McNorton, J., Agustí-Panareda, A., Arduini, G., Balsamo, G., Bousseres, N., Boussetta, S., Chericoni, M., Choulga,
 387 M., Engelen, R., & Guevara, M. (2023). An Urban Scheme for the ECMWF Integrated Forecasting System: Global
 388 Forecasts and Residential CO2 Emissions. *Journal of Advances in Modeling Earth Systems*, 15(3).
 389 <https://doi.org/10.1029/2022MS003286>
- 390 Muñoz-Sabater, J., Dutra, E., Agustí-Panareda, A., Albergel, C., Arduini, G., Balsamo, G., Boussetta, S., Choulga,
 391 M., Harrigan, S., Hersbach, H., Martens, B., Miralles, D. G., Piles, M., Rodríguez-Fernández, N. J., Zsoter, E.,
 392 Buontempo, C., & Thépaut, J.-N. (2021). ERA5-Land: a state-of-the-art global reanalysis dataset for land
 393 applications. *Earth Syst. Sci. Data*, 13(9), 4349–4383. <https://doi.org/10.5194/essd-13-4349-2021>
- 394 Rao, K., Williams, A. P., Duffenbaugh, N. S., Yebra, M., Bryant, C., & Konings, A. G. (2023). Dry Live Fuels
 395 Increase the Likelihood of Lightning-Caused Fires. *Geophysical Research Letters*, 50(15), e2022GL100975.
 396 <https://doi.org/https://doi.org/10.1029/2022GL100975>
- 397 Thonicke, K., Spessa, A., Prentice, I. C., Harrison, S. P., Dong, L., & Carmona-Moreno, C. (2010). The influence of
 398 vegetation, fire spread and fire behaviour on biomass burning and trace gas emissions: results from a process-based
 399 model. *Biogeosciences*, 7(6), 1991–2011. <https://doi.org/10.5194/bg-7-1991-2010>
- 400 Van Wagner, C. E. (1974). *Structure of the Canadian forest fire weather index*. 1333. Environment Canada,
 401 Canadian Forestry Service, Ottawa, Canada.

- 402 Wooster, M. J., Roberts, G. J., Giglio, L., Roy, D. P., Freeborn, P. H., Boschetti, L., Justice, C., Ichoku, C.,
403 Schroeder, W., Davies, D., Smith, A. M. S., Setzer, A., Csiszar, I., Strydom, T., Frost, P., Zhang, T., Xu, W., de
404 Jong, M. C., Johnston, J. M., ... San-Miguel-Ayanz, J. (2021). Satellite remote sensing of active fires: History and
405 current status, applications and future requirements. *Remote Sensing of Environment*, 267, 112694.
406 <https://doi.org/https://doi.org/10.1016/j.rse.2021.112694>
- 407 Wotton, B. M. (2009). Interpreting and using outputs from the Canadian Forest Fire Danger Rating System in
408 research applications. *Environmental and Ecological Statistics*, 16(2), 107–131. [https://doi.org/10.1007/s10651-007-](https://doi.org/10.1007/s10651-007-0084-2)
409 [0084-2](https://doi.org/10.1007/s10651-007-0084-2)
- 410 Yebra, M., Dennison, P. E., Chuvieco, E., Riaño, D., Zylstra, P., Hunt, E. R., Danson, F. M., Qi, Y., & Jurdao, S.
411 (2013). A global review of remote sensing of live fuel moisture content for fire danger assessment: Moving towards
412 operational products. *Remote Sensing of Environment*, 136, 455–468.
413 <https://doi.org/https://doi.org/10.1016/j.rse.2013.05.029>
- 414 Zhang, G., Wang, M., & Liu, K. (2021). Deep neural networks for global wildfire susceptibility modelling.
415 *Ecological Indicators*, 127, 107735. <https://doi.org/https://doi.org/10.1016/j.ecolind.2021.107735>
- 416 Zhu, Q., Li, F., Riley, W. J., Xu, L., Zhao, L., Yuan, K., Wu, H., Gong, J., & Randerson, J. (2022). Building a
417 machine learning surrogate model for wildfire activities within a global Earth system model. *Geosci. Model Dev.*,
418 15(5), 1899–1911. <https://doi.org/10.5194/gmd-15-1899-2022>
419